

JVID: Joint Video-Image Diffusion for Visual-Quality and Temporal-Consistency in Video Generation

Hadrien Reynaud
Imperial College London
London, UK
hjr119@imperial.ac.uk

Sarah Cechnicka
Imperial College London
London, UK

Matthew Baugh
Imperial College London
London, UK

Qingjie Meng
University of Birmingham
Birmingham UK

Mischa Dombrowski
Friedrich-Alexander-Universität
Erlangen-Nürnberg, DE

Bernhard Kainz
Imperial College London
London, UK
Friedrich-Alexander-Universität
Erlangen-Nürnberg, DE

Abstract

We introduce the Joint Video-Image Diffusion model (JVID), a novel approach to generating high-quality and temporally coherent videos. We achieve this by integrating two diffusion models: a Latent Image Diffusion Model (LIDM) trained on images and a Latent Video Diffusion Model (LVDM) trained on video data. Our method combines these models in the reverse diffusion process, where the LIDM enhances image quality and the LVDM ensures temporal consistency. This unique combination allows us to effectively handle the complex spatio-temporal dynamics in video generation. Our results demonstrate quantitative and qualitative improvements in producing realistic and coherent videos.

1. Introduction

Large-scale diffusion-based text-to-image models have led to remarkable improvements in image generation [2, 12, 18, 41, 42, 45, 51, 53]. They can produce high-quality, photorealistic images that follow complex text descriptions with great accuracy. Due to the success of these text-to-image generations, several works have experimented with applying them to video generation. However, generating videos is much more challenging because of their high-dimensionality and complex spatio-temporal dynamics.

Many previous works explored various generative models for video generation, such as Generative Adversarial Networks (GANs) [46, 49, 50, 56, 60, 66] and autoregressive models [8, 39, 58, 62, 64]. Nonetheless, these methods have difficulties achieving wide video mode coverage,



Figure 1. Video samples generated with our JVID model, combining both an image and a video diffusion model during sampling, to produce high quality and temporally coherent videos. Rows 1-4 are generated at 128×128 , while rows 5-8 are 64×64 .

maintaining long-term dependency, and high visual quality. Most concurrent works use diffusion models for video generation [1, 4, 13, 19–21, 25, 30, 35, 49, 59, 61, 63, 65, 69, 69]. These approaches achieve better video quality than GAN-based methods, but they come with a substantial computational cost, long training periods and long iterative sampling.

In this work, we introduce a novel Joint Video-Image Diffusion model (JVID), to generate realistic-looking and temporally-coherent videos. Examples from JVID are shown in Figure 1. We present a new sampling strat-

egy where we generate videos by mixing a video diffusion model and an image diffusion model. More specifically, two diffusion models, *i.e.*, an image model and a video model, are trained independently under the same diffusion framework. We then derive a method to sample from both models during the iterative reverse process, in order to generate videos with better visual quality. The idea is that at every denoising step, we denoise our sample with one model or the other. Because the models are trained within the same framework, they are compatible with each other, and therefore, the underlying iterative denoising process is coherent.

Prior works either train diffusion-based video models by adapting a pre-trained image diffusion model [4, 63] or train video diffusion models from scratch [15, 20, 49]. Our work utilises both an image and a video model, but their individual training regime does not matter, as long as they are both trained using the same perturbation process and noise schedule, as we detail in Section 3. Therefore, we do not require any special tricks during training, which means that any pair of pre-trained models, respecting the two previously stated conditions, would be compatible with our proposed sampling method.

Furthermore, inspired by latent diffusion models [12, 42], our method models image and video distributions in a latent space, which greatly reduces the computational cost of training and the sampling time.

The contributions of our work can be summarized as:

1. We propose a new sampling strategy to leverage the benefits of multiple diffusion models during inference.
2. We introduce two techniques (inference entropy reduction and temporal latent smoothing) to further enhance the temporal consistency in video diffusion models and,
3. we release pre-trained models to enable future research in the domain of video-image generation.

2. Related Works

2.1. Diffusion models

A diffusion model is a type of score-based generative model which learns a mapping from a Gaussian noise distribution to a target data distribution [18, 51, 53]. With stable training and great scalability, diffusion models can achieve both high sample quality and great distribution coverage [7, 40, 42, 45], leading to remarkable progress in text-to-image generation tasks. A seminal contribution in the field of diffusion models is the Denoising Diffusion Probabilistic Model (DDPM) as presented in Ho et al. [18]. This model capitalizes on the connection between Langevin dynamics [51] and denoising score matching [54], employing them to construct a weighted variational bound that serves as the basis for the optimization process. Based on the DDPM, other methods were proposed to improve the generation process. For example, the Denoising Diffusion

Implicit Model (DDIM) [52] accelerates the sampling process while maintaining the DDPM training process. The Ablated Diffusion Model (ADM) [7] uses an improved architecture and classifier guidance to achieve increased image quality. Pseudo Numerical methods for diffusion models (PNDM) [28] establishes a theoretical connection between DDPM and numerical methods. By changing the classical numerical methods to pseudo numerical methods, PNDM can accelerate the inference process while maintaining the quality of the generated images. In this work, we use DDPM sampling to benefit from the sample variety allowed by the stochastic sampling, and we rely on PNDM to train our models.

2.2. Diffusion-based Image Models

Diffusion models facilitate large-scale text-to-image generation [34, 41, 45]. However, they still suffer from major limitations *i.e.*, high memory consumption, high computational complexity and long sampling time, which is orders of magnitude longer than other generative methods due to their iterative nature. Some approaches significantly lessened these issues by applying the denoising process in the latent space rather than the RGB-space. For example, [42] trains a diffusion model in the latent space of a powerful pre-trained autoencoder, while [12] uses a pre-trained Vector Quantized Variational Autoencoder (VQ-VAE). These methods drastically reduce the memory footprint of diffusion models, resulting in faster training and inference, while keeping the quality and mode coverage of RGB-space image diffusion models. In particular, [42] opened the path for many subsequent works, thanks to its large-scale implementation known as Stable Diffusion¹. Many following works use the pre-trained Stable Diffusion weights and fine-tune them on specific tasks [5, 26, 31, 44, 63, 68], while others focused on adding more control to the generation process, given that text can be limiting [3, 6, 11, 16, 32, 33, 36, 37]. In this work, we train latent image diffusion models, as they are the most direct way to obtain the sample quality that we aim for, at an adequate computational cost. We rely on their reduced memory requirements to train models at different resolutions.

2.3. Diffusion-based Video Models

Many existing works have attempted to extend image GANs to generate videos [46, 49, 50, 56, 60, 66]. However, GANs often suffer from mode collapse and unstable training. Some other approaches use autoregressive models for video generation [8, 39, 58, 62, 64]. Although they have outperformed pure GAN-based approaches, they tend to accumulate errors over time, resulting in poor long-term dependency. Recently, several works started studying diffusion models for video generation [1, 4, 13, 19–

¹<https://stability.ai/stable-diffusion>

21, 25, 30, 35, 49, 59, 61, 63, 65, 69]. Video Diffusion Model (VDM) [20] was the first to extend an image diffusion architecture to the video domain and train jointly on both image and video data for video generation. Make-A-Video [49] leverages joint text-image priors and develops a large-scale video generation model based on text-to-image diffusion models. Imagen Video [19] builds a cascade of video diffusion models for high-resolution video generation, by using spatial and temporal super-resolution models and introduced the v-parameterization objective for diffusion models. These diffusion-based video generation methods can achieve state-of-the-art results, although they also suffer from significant computation and memory requirements. Concurrent works explore latent diffusion models for video generation. MagicVideo [69] models video distributions in a low-dimensional latent space and proposes an elaborate diffusion architecture to generate temporally coherent videos. Another work, Projected Latent Video Diffusion Models (PVDM) [67], proposes a latent video generation framework with a different video factorization technique. Specifically, it projects videos into three 2D image-like latent vectors and then uses a 2D diffusion network to model video distribution from these 2D vectors. We build on top of recent latent video diffusion models [4, 15] and show a novel way of improving their generation, combining them with an image diffusion model during the reverse diffusion process in the latent space.

3. Methods

We combine two diffusion models during the reverse diffusion process to enforce both temporal consistency and image quality. One model is a Latent Video Diffusion Model (LVDM), trained exclusively on video data. The second model is a Latent Image Diffusion Model (LIDM), trained exclusively on image data. We summarize our sampling pipeline in Figure 2. Formally, we want to sample a Gaussian noise tensor $\mathbf{s}_{t=T} \sim \mathcal{N}(\mathbf{0}, \mathbf{I})$ of shape $F \times C \times H \times W$ and denoise it into a latent video $\mathbf{v} = \mathbf{s}_{t=0}$ of the same dimensions. We apply a reverse diffusion process on $\mathbf{s}_{t=T}$, to decrease the noise level t from T to 0 in an arbitrary number of steps. During the iterative reverse diffusion process, we use either the LVDM or the LIDM to predict the noise in \mathbf{s}_t , and subtract it, following the ϵ -prediction from [18]. The LVDM enforces temporal consistency over the time axis F , while the LIDM enforces better image quality over the spatial dimensions $C \times H \times W$. In this section, we briefly present diffusion models in Section 3.1, our LIDM in Section 3.2, and our LVDM in Section 3.2. We then introduce our proposed mixture of denoising model sampling approach in Section 3.4, before detailing post-processing steps to enhance the quality of our generated videos in Section 3.5 and Section 3.6.

3.1. Denoising Diffusion Probabilistic Models

Both our latent image and latent video diffusion models are trained with a PNDM [28] scheduler, but we use DDPM [18] during inference. Here, we give an overview of the DDPM, as the inference process is where we propose our main contribution.

Given a real sample $\mathbf{s}_0 \sim q(\mathbf{s}_0)$, the forward DDPM process generates a Markov chain $\mathbf{s}_1, \dots, \mathbf{s}_T$ by progressively injecting Gaussian noise into \mathbf{s}_0 , with predetermined variance β_1, \dots, β_T , i.e.,

$$q(\mathbf{s}_t | \mathbf{s}_{t-1}) = \mathcal{N}(\mathbf{s}_t; \sqrt{1 - \beta_t} \mathbf{s}_{t-1}, \beta_t \mathbf{I}). \quad (1)$$

As t grows, \mathbf{s}_t steers towards a Gaussian distribution $\mathcal{N}(\mathbf{0}, \mathbf{I})$. Thus, the true posterior distribution of $q(\mathbf{s}_{t-1} | \mathbf{s}_t)$ can be approximated by $p_\theta(\mathbf{s}_{t-1} | \mathbf{s}_t)$ such that

$$p_\theta(\mathbf{s}_{t-1} | \mathbf{s}_t) = \mathcal{N}(\mathbf{s}_{t-1}; \mu_\theta(\mathbf{s}_t), \sigma_t^2 \mathbf{I}), \quad (2)$$

where σ_t is a known constant. In the reverse DDPM, samples $\mathbf{s}_0 \sim p_\theta(\mathbf{s}_0)$ are produced by sampling $\mathbf{s}_T \sim \mathcal{N}(\mathbf{0}, \mathbf{I})$, and progressively reducing the noise by following the inverted Markov chain from the forward DDPM. To do so, $p_\theta(\mathbf{s}_{t-1} | \mathbf{s}_t)$ is learned. Gaussian noise ϵ is added to \mathbf{s}_0 , creating samples $\mathbf{s}_t \sim q(\mathbf{s}_t | \mathbf{s}_0)$, which are used to train a model ϵ_θ , which learns to predict ϵ through a mean-squared error loss

$$\mathcal{L} = \mathbb{E}_{t \in \{1, \dots, T\}, \mathbf{s}_0 \sim q(\mathbf{s}_0), \epsilon \sim \mathcal{N}(\mathbf{0}, \mathbf{I})} [\|\epsilon - \epsilon_\theta(\mathbf{s}_t, t)\|^2]. \quad (3)$$

We derive $\mu_\theta(\mathbf{s}_t)$ in Eq. (2) from $\epsilon_\theta(\mathbf{s}_t, t)$ to model $p_\theta(\mathbf{s}_{t-1} | \mathbf{s}_t)$ [18]. Following [20], the denoising model ϵ_θ is implemented via a time-conditioned UNet [43] with residual layers [14] and self-attention layers [58]. Timesteps t are passed to ϵ_θ through a sinusoidal position embedding layer [58]. For text conditioning, a CLIP [38] text encoder and cross-attention layers are added, such that $\epsilon_\theta(\mathbf{s}_t, t, y)$ can be learned with no further modification [34, 42]. We further exploit *classifier-free guidance* [17] for enhanced conditional generation. During training, the condition y in $\epsilon_\theta(\mathbf{s}_t, t, y)$ is substituted by a null label \emptyset with a fixed probability. During sampling, the model output is

$$\hat{\epsilon}_\theta(\mathbf{s}_t, t, y) = \epsilon_\theta(\mathbf{s}_t, t, \emptyset) + g \cdot (\epsilon_\theta(\mathbf{s}_t, t, y) - \epsilon_\theta(\mathbf{s}_t, t, \emptyset)), \quad (4)$$

where g denotes the guidance scale.

Generating a new sample \mathbf{s}_0 means starting from a noise sample $\mathbf{s}_T \sim \mathcal{N}(\mathbf{0}, \mathbf{I})$ and progressively denoising it, by repeatedly calling $\epsilon_\theta(\mathbf{s}_t, t)$ with

$$\mathbf{s}_{t-1} = \frac{1}{\sqrt{\alpha_t}} \left(\mathbf{s}_t - \frac{\beta_t}{\sqrt{1 - \alpha_t}} \epsilon_\theta(\mathbf{s}_t, t) \right) + \sigma_t \mathbf{z}, \quad (5)$$

where $\mathbf{z} \sim \mathcal{N}(\mathbf{0}, \mathbf{I})$, until $t = 0$.

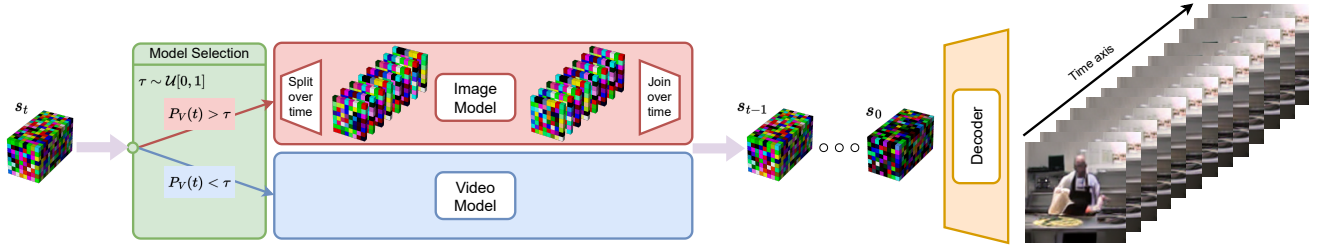


Figure 2. Our proposed mixture of denoising model sampling approach. At each step, we select one model, which is used to denoise our noise sample s_t . When the sample is fully denoised, it is decoded with the VAE decoder to reconstruct the generated video frames.

3.2. Latent Image Diffusion Models

For our text-to-image model, we take inspiration from the Stable Diffusion v1.5 model [42]. Stable Diffusion is open-source, lightweight and produces state-of-the-art image quality for many scenes and styles, while operating in a latent space. This is made possible by a pre-trained Variational Auto-Encoder (VAE), trained over billions of images [48]. The VAE encodes images of dimension $3 \times H \times W$ into latent tensors of dimension $4 \times H/8 \times W/8$. During training, the dataset samples are encoded into that latent space, and the model learns to denoise the noisy samples in the latent space. During inference, we start from latent Gaussian noise $s_T \sim N(\mathbf{0}, \mathbf{I})^{4 \times H/8 \times W/8}$ and denoise it in an arbitrary number of steps, until we reach s_0 . s_0 is then decoded using the VAE to retrieve the generated image in pixel space, as shown in Figure 2.

For our use case, because we use a different image resolution than Stable Diffusion, we train the diffusion model from scratch, in the latent space defined by the pre-trained VAE, as well as the existing CLIP text-encoder. This also allows us to make sure that both diffusion models follow the same perturbation process and noise schedule, as required by our method.

3.3. Latent Video Diffusion Models

Similarly to our LIDMs, our LVDMs are latent generative models. As such, they benefit from lower computational cost and shorter inference time. This is especially desirable for video models, where the data dimension becomes problematically large in pixel space.

Our video model differs from the image model in terms of input/output dimensions and architecture. We start from the same architecture as for the LIDM, but all 2D convolutions are replaced with 3D spatial kernels $k_s = (1, 3, 3)$, followed by temporal 3D kernels $k_t = (3, 1, 1)$. The spatial attention layers are kept, and followed by temporal attention layers. At inference, the model is given a latent noise tensor $s_T \sim N(\mathbf{0}, \mathbf{I})^{F \times 4 \times H/8 \times W/8}$. It produces a latent video s_0 which is decoded into a pixel-space video with dimension $F \times 3 \times H \times W$ by using the VAE on each indepen-

dent frame. We also experiment with a video VAE where we decode s_0 directly to leverage the correlation between all frames of the video. We find that training a video VAE on UCF-101 directly does not yield better performance due to the small size of the training dataset, as detailed in Section 4.

The LVDM is trained from scratch over a video dataset. Training from scratch allows us to (1) define an architecture that allows for metric comparison with other works, (2) suit our computational resources and (3) train a video model on the exact same perturbation process and noise schedule as our image model, as required for our sampling method. We detail the architectures and how we trained them in Section 4.

3.4. Mixture of Denoising Models

The major contribution of this work is to demonstrate that it is possible to combine diffusion models during the reverse diffusion process by selecting one noise prediction model at each time step. This idea allows to leverage models with different capabilities, producing better samples benefitting from all models' strengths. To enable this, the models need to share the same diffusion training framework. This comprises the nature of the perturbation process, which is usually the addition of Gaussian noise, as well as the same scheduling approach, to scale the perturbation at every step. Here, we train the models in the PNDM framework to perform ϵ -prediction [18]. The ϵ -prediction means that the neural network learns to predict the noise which has to be removed from its input.

Formally, given a real sample $s_0 \sim q(s_0)$, the set of all noisy samples \mathcal{S} and its subsets of noisy samples at any given timestep \mathcal{S}_t are defined as:

$$\mathcal{S}_t = \{s_t | s_t = s_0 + z_t, z_t \sim \mathcal{N}(\mathbf{0}, \sigma_t^2 \mathbf{I})\}, \quad (6)$$

$$\mathcal{S} = \{\mathcal{S}_t | t \in \{0, \dots, T\}\}, \quad (7)$$

where z_t represents the noise added to the sample s_0 at time t , and σ_t^2 is the variance of the noise at time t .

Let $\mathcal{D} = \{\mathcal{D}_1, \mathcal{D}_2, \dots, \mathcal{D}_k\}$ be the set of denoising models. Assuming that for all timesteps $t \in \{0, \dots, T\}$, any

denoising model $\mathcal{D}_i, \mathcal{D}_j \in \mathcal{D}$ is trained on the same subset \mathcal{S}_t , then any model \mathcal{D}_i is interchangeable with \mathcal{D}_j in the reverse diffusion process, as they both produce outputs in the same subset \mathcal{S}_t . In practice, this only holds if all the models are good enough to generate samples close to the true distribution of \mathcal{S}_t .

In this work, we specifically focus on demonstrating that approach by combining an LIDM and an LVDM. As suggested by above, any group of diffusion models that share the same noise inputs and outputs distributions are compatible, regardless of their conditioning. By demonstrating this among models trained on vastly different tasks, *i.e.*, video versus image, we empirically demonstrate that this holds even in complex cases.

While this approach works out of the box, it requires some tuning at inference. To find out which proportion of each model we want, as well as how to best take advantage of each, we explore various parameters for our model-selection function, which we describe in Section 4. We usually start by sampling only from the video model for a few steps, to ensure some temporal consistency, before deciding between calling one model or the other, depending on our selection function parameters. Switching from video to image works by merging the batch and time dimensions. This enables the denoising of all frames separately when calling the image model. Conversely, to switch our images to a video, we undo the merging and pass the reshaped tensor into the video model to predict the noise of the entire video.

3.5. Inference Entropy Reduction

Combining video and image models in a DDPM setting leads to an obvious limitation when using Equation (5) to sample from the models. When sampling from the image model, the term z adds noise to the samples with no consideration for the temporal consistency. To mitigate this, we define a new way of sampling z ;

$$z_{\text{shared}} \sim \mathcal{N}(\mathbf{0}, r\mathbf{I}), \quad z_{\text{ind}}^f \sim \mathcal{N}(\mathbf{0}, (1-r)\mathbf{I}), \quad (8)$$

$$z^f = z_{\text{shared}} + z_{\text{ind}}^f, \text{ where } z^f \in \mathcal{R}^{1 \times C \times H \times W}, \quad (9)$$

where z^f is the noise we add to the samples generated by the image model, f is the index of the frame on the time axis, z_{shared} is the noise shared across all frames and z_{ind}^f is the independent noise added to each frame. $r \in [0, 1]$ sets the ratio between the amount of shared and independent noise for all frames.

Additionally, we also explore reducing the overall entropy, *i.e.*, scaling down z . In Equation (5), z is scaled by a factor σ_t , which defines the amount of stochasticity added back into the sample after it is denoised. We add a factor γ to scale z such that $\sigma_t \cdot z$ becomes $\gamma \cdot \sigma_t \cdot z$.

We note that a similar approach has been explored in [10]. Our approach is substantially different, as we

control the noise only at inference and only for the time-agnostic image model, leaving the video model untouched. Our Equation (9) is also ratio-based and bounded, which makes it more interpretable.

3.6. Temporal Latent Smoothing

A major problem in current state-of-the-art diffusion models [63] is the flickering that occurs along the time axis. Some works have explored potential solutions [24] but we design a new approach, better suited to reduce flickering directly in the latent space.

Our proposed approach for a latent smoothing algorithm starts by considering the latent variables of each channel separately and computes the average of each spatial position value over the time axis, which we denote $\mu_{c,h,w}$. Following this, we compute the standard deviation of $\mu_{c,h,w}$ over h, w , denoted as σ_c , which acts as a measure of how much spatial variation there is in the video within each channel. We then calculate the absolute difference between each voxel and the corresponding $\mu_{c,h,w}$ for that location, giving us a measure of how much that voxel is deviating from its average for each frame, $\Delta_{c,f,h,w}$. We can then normalize these measures of variation using σ_c , and sum across the channels to get a single value for how much that pixel is varying within that frame in comparison to others. A hyperparameter c is then used as a threshold to determine whether the normalized variation is small enough to be close to the mean value of that location. Latent variables with a variation measure below this threshold are therefore replaced with the mean latent code $\mu_{c,h,w}$, smoothing areas that are unlikely to belong to the action in the video.

4. Experiments

In this section, we describe in detail how we trained all the models, starting with the diffusion models and the video autoencoder. We evaluate our ideas on the UCF-101 dataset and show the feasibility of our approach, as well as the impact of each of our post-processing steps on the final video sample quality.

4.1. Model training

Dataset We train all our models on the UCF-101 dataset [55]. The dataset consists of 13,320 videos of humans performing 101 different actions in the wild. All the videos have a resolution of 320×240 pixels and a frame rate of 25 frames per second (fps) for the majority. Each video belongs to one of the 101 classes. For our experiments, we resample the videos to 3 resolutions, 64×64 , 128×128 and 256×256 . We apply 240×240 center-cropping on all the frames before resizing them to the desired resolution. We also fix the frame rate to 10 fps for all videos. All our video models are trained to generate 16 frames-long videos. We

Architecture	Image	Video
# channels	256	256
Channel multiplier	[1,2,3,4]	[1,2,3,4]
# residual blocks	2	2
# channels in att. heads	64	64
# attention heads	8	8
Cross-Attention	[0,1,1,1]	[0,1,1,1]

Table 1. Model architectures. The layers in the image model are all convolutional 2D layers and 2D cross-attention layers while the layers in the video model are all 3D and contain additional Temporal-Attention layers.

pre-compute the latent image representations at each resolution using the pre-trained VAE from Stable Diffusion 1.5² to speed up training.

Architectures For all our diffusion models, we use the diffusers library³. Our image models and video models share the same architecture hyperparameters, as described in Table 1. For the image model, we use a 2D downsampling layer as our first block in our UNet, followed by 3 cross-correlation blocks. We use the same strategy for the video model, but all the layers are 3D and use temporal-attention. For our autoencoder we adopt the video VAE proposed by [15]. However, since the latents are directly generated by our diffusion models we only train the decoder.

Text conditioning For text conditioning, we use the CLIP [38] tokenizer and text encoder. CLIP creates sequences of embeddings of dimension 768, which we inject into the cross-correlation layers of our models. The text we encode for the UCF-101 dataset is the name of the classes with little processing. All the class names describe a scene, but there is no rule as to how this is written, resulting in some actions described as, *e.g.*, ‘ApplyEyeMakeup’ and some object names as, *e.g.*, ‘ParallelBars’. We apply a simple function to split the words based on the capital letters, resulting in sentences like ‘apply eye makeup’ and ‘parallel bars’ to which we randomly prepend either ‘A human’, ‘A person’ or ‘Someone’. While this technique would achieve subpar results if we were using a pretrained text-conditioned model, it does not impact our models as we train and infer over the same conditionings.

For completeness, we also explore our models in an unconditional setting. This is achieved by computing the embedding for the empty sentence with the text encoder, and using it as ‘no conditioning’.

Training For all models, we use the AdamW [29] optimizer, with a constant learning rate of $1e-4$ after 500 steps of initial warm up. We use a 30% probability of dropping

²<https://huggingface.co/runwayml/stable-diffusion-v1-5>

³<https://huggingface.co/docs/diffusers/index>

the prompt conditioning and a noise offset of 0.1^4 for the noise samples.

For the latent image models, we use a batch size of 1024, split over $8 \times$ A100 80Gb and no gradient accumulation. Each model is trained from scratch, for 100,000 optimization steps, resulting in training times of roughly 70, 85 and 185 GPU-hours, for the 64^2 , 128^2 and 256^2 models respectively.

For the latent video models, we train the models consecutively. We start with the 64^2 model, trained for 100,000 steps, with a batch size of 1024, over $64 \times$ A100 80Gb. After the low-resolution 64^2 model is trained, we re-use the weights and continue training on the 128^2 resolution for an additional 50,000 steps with the exact same configuration. Finally, we train the 256^2 model starting from the 128^2 model. Due to training instability leading to NaN-values, we increase the learning to $2e-4$ and the ϵ value in the AdamW optimizer from $1e-8$ to $1e-04$. For this model, we reduce the per-device batch size by 2 and set gradient accumulation to 2, in order to keep a global batch size of 1024. The model is trained for another 50,000 steps. This results in 2400 GPU-hours for the 64^2 model, 1500 additional hours for 128^2 model and another 2000 for the final 50,000 steps at resolution 256^2 .

4.2. Models evaluation

For each model, we perform iterative hyperparameter searches. For the video models, we keep the hyperparameters lowering the Fréchet Video Distance (FVD) the most, while for the image model, we focus on the Fréchet Inception Distance (FID). The first hyperparameter search focuses on the best combination of guidance scale and sampler. We evaluate guidance scales [0, 1, 2, 4, 6, 8, 10] and samplers DDPM, DDIM and PNDM. After establishing the best guidance scale and sampler, we look for the best number of sampling steps, evaluating 20, 30, 40, 50, 60, 75, 100 and 200 steps. We find that, for all models, the combination of the DDPM scheduler, guidance scale 2.0 and 50 sampling steps either yields the best results or falls within the margin of error. We therefore use these parameters for all the models. We then explore the model selection for the mixture of denoising models, which we describe in more detail in Section 4.3. Once we have defined the best way to select the models, we move on to the post-processing. First, we explore whether reducing the entropy in the reverse diffusion process (Equation (5)) helps to better maintain the temporal consistency. We check the metrics for parameter γ (Section 3.5), as well as the ratio r for both the video model (r_v) and the image model (r_i). We test $\gamma \in [0.5, 0.2, 0.1, 0.05, 0.02, 0.01]$ and $r_v, r_i \in [0.2, 0.4, 0.6, 0.8, 1.0]$. We discover that using correlated noise does not help with metrics, thus r_v and r_i are set to

⁴<https://www.crosslabs.org/blog/diffusion-with-offset-noise>

Resolution	64 × 64			128 × 128			256 × 256		
Method	FID↓	FVD↓	IS↑	FID↓	FVD↓	IS↑	FID↓	FVD↓	IS↑
Image AE [42]	57.09	758.96	4.46	67.12	246.46	4.41	75.11	83.00	4.32
Video AE	63.86	877.04	4.24	68.68	298.71	4.33	83.49	440.61	4.13
Video Model	23.94	885.68	8.28 \pm 0.26	32.63	1057.34	10.80 \pm 0.41	71.10	1590.81	7.84 \pm 0.17
Image Model	32.97	1631.38	7.56 \pm 0.09	17.09	1840.10	11.30 \pm 0.14	14.60	2072.09	14.51 \pm 0.12
V+I Model	33.8	1105.39	7.93 \pm 0.18	31.31	1145.4	11.16 \pm 0.30	31.02	1808.23	12.32 \pm 0.26
+Red. Entropy	31.89	1077.02	7.91 \pm 0.20	31.70	1065.15	11.10 \pm 0.40	49.37	1838.88	10.71 \pm 0.71
+Smoothing	31.79	1044.23	7.77 \pm 0.18	31.44	1037.81	11.25 \pm 0.42	50.95	1872.71	9.84 \pm 0.19

Table 2. Ablation study of all our models. We evaluate each model independently, before progressively adding our improvements. The best performing video generation pipeline is highlighted in grey.

Method	FVD ₁₆
MoCoGAN [57]	2886.9
+ StyleGAN2 backbone [50]	1821.4
MoCoGAN-HD [56]	1729.6
VideoGPT [64]†	2880.6
DIGAN [66]	1630.2
StyleGAN-V [50]	1431.0
JVID (ours)	1590.81

Table 3. We compare our method to StyleGAN-V [50] recomputed metrics following the StyleGAN-V protocol on resolution 256².

0 for all models. For γ , we find that the 64² model works better with $\gamma = 0.02$, the 128² model with $\gamma = 0.1$ and the 256² model with $\gamma = 1.0$. For the smoothing post-processing, we explore three algorithms: Gaussian smoothing, uniform smoothing, and the custom-designed approach presented in Section 3.6. We find that our smoothing strategy works the best, with a smoothing factor of 2 for all models. All experiments are seeded, to enable reproducibility and a fair comparison.

Regarding metric computation, we follow the StyleGAN-V protocol [50]. We compute the FID over 50,000 images, where the images are part of 16-frames long videos, the FVD₁₆ over 2048 videos and the Inception Score (IS) over 10 × 5,000 images, and report the mean and standard deviation. We note that StyleGAN-V [50] re-evaluated some of the models we compare against. To make sure to provide a fair comparison, we compare our results to both the metrics claimed by each individual work, as well as the metrics recomputed by StyleGAN-V. We report all metrics in Table 3, Table 4 and Table 5, and show qualitative results in Figure 1 and Figure 4.

Method	Res.	FVD (↓)	IS (↑)
TGANv2 [47]	128	-	26.60 \pm 0.47
DIGAN [66]	128	577 \pm 22	32.70
MoCoGAN-HD [56]	256	700 \pm 24	33.95 \pm 0.25
CogVideo [22]	160	626	50.46
VDM [20]	64	-	57.80 \pm 1.3
TATS-base [9]	128	278 \pm 11	79.28 \pm 0.38
Make-A-Video [49]	256	81.25	82.55
JVID (ours)	64	885.68	8.28 \pm 0.26
JVID (ours)	128	1037.81	11.25 \pm 0.42
JVID (ours)	256	1590.81	7.84 \pm 0.17

Table 4. Text-conditioned video generation on UCF-101. All models are trained or fine-tuned on UCF-101.

Method	Res.	FVD (↓)	IS (↑)
TGAN [46]	128	-	15.83 \pm 1.18
LDVD-GAN [23]	64	-	22.91 \pm 1.19
VideoGPT [64]	128	-	24.69 \pm 0.30
MoCoGAN-HD [57]	256	838	32.36
DIGAN [66]	128	655 \pm 22	29.71 \pm 0.53
CCVS [27]	128	386 \pm 15	24.47 \pm 1.13
StyleGAN-V [50]	256	-	23.94 \pm 0.73
VDM [20]	64	-	57.00 \pm 0.62
TATS [9]	128	430 \pm 18	57.63 \pm 0.73
PYoCo [10]	64	310 \pm 13	60.01 \pm 0.51
JVID (ours)	64	2143.16	6.02 \pm 0.15
JVID (ours)	128	1257.07	10.25 \pm 0.39
JVID (ours)	256	2681.54	7.16 \pm 0.19

Table 5. Unconditional video generation on UCF-101.

4.3. Mixture of Denoising Models

The main contribution of this work is the demonstration that different diffusion models, trained on identical input and output distributions, are compatible during the reverse diffusion process. Here we present the reasoning behind our mixing strategy. It decides which model to call at which step, in the reverse diffusion process. When mixing a time-aware video and a time-agnostic image model, we consider that the video model will take a noisy input and denoise it with the objective of enforcing temporal consistency, while the image model will denoise the same noisy input and push it towards better image quality. When denoising with our image model, the model is deterministic, but ignores the temporal consistency, resulting in samples that slowly degrade the images’ coherence over the time axis. Thus, the idea is to sample from both models at optimal timesteps to maintain both temporal consistency and image quality. From early experimentation, we notice that starting by sampling exclusively from the video model, is central to setting up a latent representation with a good temporal consistency. After that, we randomly select the model which we sample from, given a probability $P_V(t)$ to sample from the video model. It appears that abruptly altering the model sampling probability causes a degradation in video quality. Therefore, we opt for a gradual linear interpolation between the initial and final values of $P_V(t)$. It also turns out that sampling only from the image model for a given amount of final steps led to noticeable damage to the temporal consistency, and as such some probability of sampling from the video model is kept for the entire sampling duration. We opt for a piece-wise affine function, to allow for different probability gradients, as shown in Figure 3. This approach was selected to enhance flexibility during the sampling process, enabling the image model to exert a greater influence in the initial stages without prematurely diminishing the probability of the video model’s contribution. This concept can be formally expressed as

$$P_V(t) = \begin{cases} 1.0, & \text{if } t \geq t_v \\ 1 + \left(\frac{t-t_v}{t_e-t_v}\right) \cdot (p_e - 1), & \text{if } t_v > t \geq t_e \\ p_e + \left(\frac{t-t_e}{1-t_e}\right) \cdot (p_f - p_e), & \text{otherwise.} \end{cases}$$

We report the best model section hyperparameters for each resolution in Table 6.

5. Discussion

We acknowledge that the models used in this work do not beat state-of-the-art approaches. This is due to the considerable amount of compute necessary to match these models’ performance. For example, Make-A-Video [49] reaches an FVD of 81.25. However, their model is pre-trained over millions of samples before being fine-tuned on UCF-101,

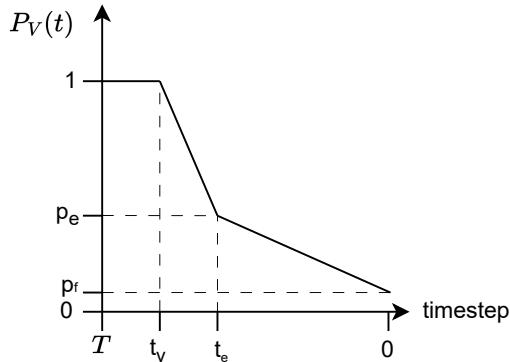


Figure 3. Model selection probability function. Parameters t_v, t_e, p_e, p_f are determined empirically.

Resolution	t_v	t_e	p_e	p_f
64×64	0.2	0.7	0.3	0.3
128×128	0.4	0.7	0.4	0.1
256×256	0.1	0.6	0.2	0.1

Table 6. Best model selection hyperparameters.

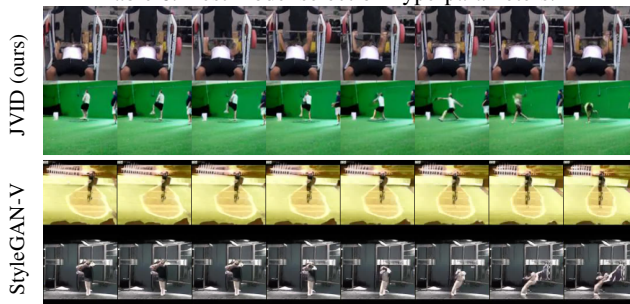


Figure 4. Our JVID model (top two rows) demonstrates higher image quality and temporal consistency compared to StyleGAN-V [50] (bottom two rows).

which is not something usually achievable with academic resources. Additionally, the very few papers which do release their models and code were not immediately compatible with our method, requiring us to fully retrain all our models.

When fairly comparing our work, especially with the results from Table 3, we come close to the state-of-the-art when training on similar amounts of data. This leads us to believe that our mixture of denoising models should be explored further in more settings, and at a greater scale.

Environmental Impact. Our work involved substantial energy consumption, utilizing 8,000 hours of A40 energy and 24,000 hours of A100 energy, cumulatively amounting to a significant 12,000 kilowatt-hours of electricity used. A Tesla Model 3 could be powered for 55,800 miles with this amount of energy. This level of energy usage underscores

the importance of considering the environmental impact of such projects, particularly in terms of their carbon footprint and contribution to energy consumption. Therefore, we will publish our model weights together with all the code so that any subsequent work can continue from this point.

6. Conclusion

This work presents a new way to combine diffusion models during inference. Our results show that we can indeed generate samples while using two independently trained diffusion models. Additionally, our approach has minimal requirements and should synergize with many existing conditioning approaches, which is what we intend to explore in future works.

References

- [1] Jie An, Songyang Zhang, Harry Yang, Sonal Gupta, Jia-Bin Huang, Jiebo Luo, and Xi Yin. Latent-shift: Latent diffusion with temporal shift for efficient text-to-video generation. *arXiv preprint arXiv:2304.08477*, 2023. 1, 2
- [2] Yogesh Balaji, Seungjun Nah, Xun Huang, Arash Vahdat, Jiaming Song, Qinsheng Zhang, Karsten Kreis, Miika Aittala, Timo Aila, Samuli Laine, Bryan Catanzaro, and et al. ediff-i: Text-to-image diffusion models with an ensemble of expert denoisers. *arXiv preprint arXiv:2211.01324*, 2022. 1
- [3] Omer Bar-Tal, Dolev Ofri-Amar, Rafail Fridman, Yoni Kasten, and Tali Dekel. Text2live: Text-driven layered image and video editing. In *ECCV*. Springer, 2022. 2
- [4] Andreas Blattmann, Robin Rombach, Huan Ling, Tim Dockhorn, Seung Wook Kim, Sanja Fidler, and Karsten Kreis. Align your latents: High-resolution video synthesis with latent diffusion models. In *Proceedings of the IEEE/CVF Conference on Computer Vision and Pattern Recognition*, pages 22563–22575, 2023. 1, 2, 3
- [5] Tim Brooks, Aleksander Holynski, and Alexei A Efros. Instructpix2pix: Learning to follow image editing instructions. In *CVPR*, 2023. 2
- [6] Duygu Ceylan, Chun-Hao Huang, and Niloy J Mitra. Pix2video: Video editing using image diffusion. *arXiv:2303.12688*, 2023. 2
- [7] Prafulla Dhariwal and Alexander Nichol. Diffusion models beat gans on image synthesis. *Advances in Neural Information Processing Systems*, 34, 2021. 2
- [8] Patrick Esser, Robin Rombach, and Bjorn Ommer. Taming transformers for high-resolution image synthesis. In *Proceedings of the IEEE/CVF Conference on Computer Vision and Pattern Recognition*, 2021. 1, 2
- [9] Songwei Ge, Thomas Hayes, Harry Yang, Xi Yin, Guan Pang, David Jacobs, Jia-Bin Huang, and Devi Parikh. Long video generation with time-agnostic vqgan and time-sensitive transformer. *arXiv preprint arXiv:2204.03638*, 2022. 7
- [10] Songwei Ge, Seungjun Nah, Guilin Liu, Tyler Poon, Andrew Tao, Bryan Catanzaro, David Jacobs, Jia-Bin Huang, Ming-Yu Liu, and Yogesh Balaji. Preserve your own correlation: A noise prior for video diffusion models. In *ICCV*, 2023. 5, 7
- [11] Songwei Ge, Taesung Park, Jun-Yan Zhu, and Jia-Bin Huang. Expressive text-to-image generation with rich text. *arXiv preprint arXiv:2304.06720*, 2023. 2
- [12] Shuyang Gu, Dong Chen, Jianmin Bao, Fang Wen, Bo Zhang, Dongdong Chen, Lu Yuan, and Baining Guo. Vector quantized diffusion model for text-to-image synthesis. In *CVPR*, 2022. 1, 2
- [13] William Harvey, Saeid Naderiparizi, Vaden Masrani, Christian Weilbach, and Frank Wood. Flexible diffusion modeling of long videos. *arXiv preprint arXiv:2205.11495*, 2022. arXiv:2205.11495. 1, 2
- [14] Kaiming He, Xiangyu Zhang, Shaoqing Ren, and Jian Sun. Deep residual learning for image recognition. In *Proceedings of the IEEE conference on computer vision and pattern recognition*, pages 770–778, 2016. 3
- [15] Yingqing He, Tianyu Yang, Yong Zhang, Ying Shan, and Qifeng Chen. Latent video diffusion models for high-fidelity video generation with arbitrary lengths. *arXiv preprint arXiv:2211.13221*, 2022. 2, 3, 6
- [16] Amir Hertz, Ron Mokady, Jay Tenenbaum, Kfir Aberman, Yael Pritch, and Daniel Cohen-Or. Prompt-to-prompt image editing with cross attention control. *arXiv preprint arXiv:2208.01626*, 2022. 2
- [17] Jonathan Ho and Tim Salimans. Classifier-free diffusion guidance. *arXiv preprint arXiv:2207.12598*, 2022. arXiv:2207.12598. 3
- [18] Jonathan Ho, Ajay Jain, and Pieter Abbeel. Denoising diffusion probabilistic models. In *NeurIPS*, 2020. 1, 2, 3, 4
- [19] Jonathan Ho, William Chan, Chitwan Saharia, Jay Whang, Ruiqi Gao, Alexey Gritsenko, Diederik P Kingma, Ben Poole, Mohammad Norouzi, David J Fleet, et al. Imagen video: High definition video generation with diffusion models. *arXiv preprint arXiv:2210.02303*, 2022. arXiv:2210.02303. 1, 2, 3
- [20] Jonathan Ho, Tim Salimans, Alexey Gritsenko, William Chan, Mohammad Norouzi, and David J Fleet. Video diffusion models. *arXiv preprint arXiv:2204.03458*, 2022. arXiv:2204.03458. 2, 3, 7
- [21] Tobias Hoeppe, Arash Mehrjou, Stefan Bauer, Didrik Nielsen, and Andrea Dittadi. Diffusion models for video prediction and infilling. *arXiv preprint arXiv:2206.07696*, 2022. 1, 3
- [22] Wenyi Hong, Ming Ding, Wendi Zheng, Xinghan Liu, and Jie Tang. Cogvideo: Large-scale pretraining for text-to-video generation via transformers. *arXiv preprint arXiv:2205.15868*, 2022. 7
- [23] Emmanuel Kahembwe and Subramanian Ramamoorthy. Lower dimensional kernels for video discriminators. *Neural Networks*, 2020. 7
- [24] Johanna Karras, Aleksander Holynski, Ting-Chun Wang, and Ira Kemelmacher-Shlizerman. Dreampose: Fashion image-to-video synthesis via stable diffusion. *arXiv preprint arXiv:2304.06025*, 2023. 5
- [25] Levon Khachatryan, Andranik Movsisyan, Vahram Tadevosyan, Roberto Henschel, Zhangyang Wang, Shant

- Navasardyan, and Humphrey Shi. Text2video-zero: Text-to-image diffusion models are zero-shot video generators. In *Proceedings of the IEEE/CVF International Conference on Computer Vision (ICCV)*, 2023. 1, 3
- [26] Nupur Kumari, Bingliang Zhang, Richard Zhang, Eli Shechtman, and Jun-Yan Zhu. Multi-concept customization of text-to-image diffusion. *arXiv preprint arXiv:2212.04488*, 2022. 2
- [27] Guillaume Le Moing, Jean Ponce, and Cordelia Schmid. Ccvs: Context-aware controllable video synthesis. *NeurIPS*, 2021. 7
- [28] Luping Liu, Yi Ren, Zhijie Lin, and Zhou Zhao. Pseudo numerical methods for diffusion models on manifolds. *arXiv preprint arXiv:2202.09778*, 2022. 2, 3
- [29] Ilya Loshchilov and Frank Hutter. Decoupled weight decay regularization. *arXiv preprint arXiv:1711.05101*, 2017. 6
- [30] Zhengxiong Luo, Dayou Chen, Yingya Zhang, Yan Huang, Liang Wang, Yujun Shen, Deli Zhao, Jingren Zhou, and Tieniu Tan. Videofusion: Decomposed diffusion models for high-quality video generation. In *CVPR*, 2023. 1, 3
- [31] Yue Ma, Yingqing He, Xiaodong Cun, Xintao Wang, Ying Shan, Xiu Li, and Qifeng Chen. Follow your pose: Pose-guided text-to-video generation using pose-free videos. *arXiv preprint arXiv:2304.01186*, 2023. 2
- [32] Chenlin Meng, Yutong He, Yang Song, Jiaming Song, Jiajun Wu, Jun-Yan Zhu, and Stefano Ermon. Sdedit: Guided image synthesis and editing with stochastic differential equations. In *ICLR*, 2022. 2
- [33] Eyal Molad, Eliahu Horwitz, Dani Valevski, Alex Rav Acha, Yossi Matias, Yael Pritch, Yaniv Leviathan, and Yedid Hoshen. Video diffusion models are general video editors. *arXiv preprint arXiv:2302.01329*, 2023. 2
- [34] Alex Nichol, Prafulla Dhariwal, Aditya Ramesh, Pranav Shyam, Pamela Mishkin, Bob McGrew, Ilya Sutskever, and Mark Chen. Glide: Towards photorealistic image generation and editing with text-guided diffusion models. *arXiv preprint arXiv:2112.10741*, 2021. 2, 3
- [35] Yaniv Nikankin, Niv Haim, and Michal Irani. Sinfusion: Training diffusion models on a single image or video. *arXiv preprint arXiv:2211.11743*, 2022. 1, 3
- [36] Gaurav Parmar, Krishna Kumar Singh, Richard Zhang, Yijun Li, Jingwan Lu, and Jun-Yan Zhu. Zero-shot image-to-image translation. *arXiv preprint arXiv:2302.03027*, 2023. 2
- [37] Chenyang Qi, Xiaodong Cun, Yong Zhang, Chenyang Lei, Xintao Wang, Ying Shan, and Qifeng Chen. Fatezero: Fusing attentions for zero-shot text-based video editing. *arXiv preprint arXiv:2303.09535*, 2023. 2
- [38] Alec Radford, Jong Wook Kim, Chris Hallacy, Aditya Ramesh, Gabriel Goh, Sandhini Agarwal, Girish Sastry, Amanda Askell, Pamela Mishkin, Jack Clark, Gretchen Krueger, and Ilya Sutskever. Learning transferable visual models from natural language supervision. In *ICML*, 2021. 3, 6
- [39] Ruslan Rakhimov, Denis Volkhonskiy, Alexey Artemov, Denis Zorin, and Evgeny Burnaev. Latent video transformer. *arXiv preprint arXiv:2006.10704*, 2020. 1, 2
- [40] Aditya Ramesh, Mikhail Pavlov, Gabriel Goh, Scott Gray, Chelsea Voss, Alec Radford, Mark Chen, and Ilya Sutskever. Zero-shot text-to-image generation. In *International Conference on Machine Learning*, pages 8821–8831. PMLR, 2021. 2
- [41] Aditya Ramesh, Prafulla Dhariwal, Alex Nichol, Casey Chu, and Mark Chen. Hierarchical text-conditional image generation with clip latents. *arXiv preprint arXiv:2204.06125*, 2022. 1, 2
- [42] Robin Rombach, Andreas Blattmann, Dominik Lorenz, Patrick Esser, and Bjorn Ommer. High-resolution image synthesis with latent diffusion models. In *CVPR*, 2022. arXiv:2112.10752. 1, 2, 3, 4, 7
- [43] Olaf Ronneberger, Philipp Fischer, and Thomas Brox. U-net: Convolutional networks for biomedical image segmentation. In *Medical Image Computing and Computer-Assisted Intervention—MICCAI 2015: 18th International Conference, Munich, Germany, October 5–9, 2015, Proceedings, Part III*. Springer, 2015. arXiv:1505.04597. 3
- [44] Nataniel Ruiz, Yuanzhen Li, Varun Jampani, Yael Pritch, Michael Rubinstein, and Kfir Aberman. Dreambooth: Fine tuning text-to-image diffusion models for subject-driven generation. *arXiv preprint arXiv:2208.12242*, 2022. 2
- [45] Chitwan Saharia, William Chan, Saurabh Saxena, Lala Li, Jay Whang, Emily Denton, Seyed Kamyar Seyed Ghasemipour, Burcu Karagol Ayan, S Sara Mahdavi, Rapha Gontijo Lopes, et al. Photorealistic text-to-image diffusion models with deep language understanding. *arXiv preprint arXiv:2205.11487*, 2022. arXiv:2205.11487. 1, 2
- [46] Masaki Saito, Eiichi Matsumoto, and Shunta Saito. Temporal generative adversarial nets with singular value clipping. In *ICCV*, 2017. 1, 2, 7
- [47] Masaki Saito, Shunta Saito, Masanori Koyama, and Sotuke Kobayashi. Train sparsely, generate densely: Memory-efficient unsupervised training of high-resolution temporal gan. *IJCV*, 128, 2020. 7
- [48] Christoph Schuhmann, Romain Beaumont, Richard Vencu, Cade Gordon, Ross Wightman, Mehdi Cherti, Theo Coombes, Aarush Katta, Clayton Mullis, Mitchell Wortsman, et al. Laion-5b: An open large-scale dataset for training next generation image-text models. *Advances in Neural Information Processing Systems*, 35:25278–25294, 2022. 4
- [49] Uriel Singer, Adam Polyak, Thomas Hayes, Xi Yin, Jie An, Songyang Zhang, Qiyuan Hu, Harry Yang, Oron Ashual, Oran Gafni, et al. Make-a-video: Text-to-video generation without text-video data. *arXiv preprint arXiv:2209.14792*, 2022. arXiv:2209.14792. 1, 2, 3, 7, 8
- [50] Ivan Skorokhodov, Sergey Tulyakov, and Mohamed Elhoseiny. Stylegan-v: A continuous video generator with the price, image quality and perks of stylegan2. *arXiv preprint arXiv:2112.14683*, 2021. 1, 2, 7, 8
- [51] Jascha Sohl-Dickstein, Eric Weiss, Niru Maheswaranathan, and Surya Ganguli. Deep unsupervised learning using nonequilibrium thermodynamics. In *International Conference on Machine Learning*. PMLR, 2015. arXiv:1503.03585. 1, 2
- [52] Jiaming Song, Chenlin Meng, and Stefano Ermon.

- Denoising diffusion implicit models. *arXiv preprint arXiv:2010.02502*, 2020. arXiv:2010.02502. [2](#)
- [53] Yang Song and Stefano Ermon. Generative modeling by estimating gradients of the data distribution. *Advances in neural information processing systems*, 32, 2019. [1](#), [2](#)
- [54] Yang Song, Jascha Sohl-Dickstein, Diederik P Kingma, Abhishek Kumar, Stefano Ermon, and Ben Poole. Score-based generative modeling through stochastic differential equations. *arXiv preprint arXiv:2011.13456*, 2020. arXiv:2011.13456. [2](#)
- [55] Khurram Soomro, Amir Roshan Zamir, and Mubarak Shah. Ucf101: A dataset of 101 human actions classes from videos in the wild. *arXiv preprint arXiv:1212.0402*, 2012. [5](#)
- [56] Yu Tian, Jian Ren, Menglei Chai, Kyle Olszewski, Xi Peng, Dimitris N Metaxas, and Sergey Tulyakov. A good image generator is what you need for high-resolution video synthesis. In *ICLR*, 2021. [1](#), [2](#), [7](#)
- [57] Sergey Tulyakov, Ming-Yu Liu, Xiaodong Yang, and Jan Kautz. Mocogan: Decomposing motion and content for video generation. In *CVPR*, 2018. [7](#)
- [58] Ashish Vaswani, Noam Shazeer, Niki Parmar, Jakob Uszkoreit, Llion Jones, Aidan N Gomez, Łukasz Kaiser, and Illia Polosukhin. Attention is all you need. *Advances in neural information processing systems*, 30, 2017. [1](#), [2](#), [3](#)
- [59] Vikram Voleti, Alexia Jolicoeur-Martineau, and Christopher Pal. Masked conditional video diffusion for prediction, generation, and interpolation. *arXiv preprint arXiv:2205.09853*, 2022. [1](#), [3](#)
- [60] Carl Vondrick, Hamed Pirsiavash, and Antonio Torralba. Generating videos with scene dynamics. In *NIPS*, 2016. [1](#), [2](#)
- [61] Wenjing Wang, Huan Yang, Zixi Tuo, Huiguo He, Junchen Zhu, Jianlong Fu, and Jiaying Liu. Videofactory: Swap attention in spatiotemporal diffusions for text-to-video generation. *arXiv preprint arXiv:2305.10874*, 2023. [1](#), [3](#)
- [62] Dirk Weissenborn, Oscar Tackstrom, and Jakob Uszkoreit. Scaling autoregressive video models. *arXiv preprint arXiv:1906.02634*, 2019. [1](#), [2](#)
- [63] Jay Zhangjie Wu, Yixiao Ge, Xintao Wang, Stan Weixian Lei, Yuchao Gu, Yufei Shi, Wynne Hsu, Ying Shan, Xiaohu Qie, and Mike Zheng Shou. Tune-a-video: One-shot tuning of image diffusion models for text-to-video generation. In *Proceedings of the IEEE/CVF International Conference on Computer Vision*, pages 7623–7633, 2023. [1](#), [2](#), [3](#), [5](#)
- [64] Wilson Yan, Yunzhi Zhang, Pieter Abbeel, and Aravind Srinivas. Videogpt: Video generation using vq-vae and transformers. *arXiv preprint arXiv:2104.10157*, 2021. [1](#), [2](#), [7](#)
- [65] Ruihan Yang, Prakhar Srivastava, and Stephan Mandt. Diffusion probabilistic modeling for video generation. *arXiv preprint arXiv:2203.09481*, 2022. arXiv:2203.09481. [1](#), [3](#)
- [66] Sihyun Yu, Jihoon Tack, Sangwoo Mo, Hyunsu Kim, Junho Kim, Jung-Woo Ha, and Jinwoo Shin. Generating videos with dynamics-aware implicit generative adversarial networks. In *ICLR*, 2022. [1](#), [2](#), [7](#)
- [67] Sihyun Yu, Kihyuk Sohn, Subin Kim, and Jinwoo Shin. Video probabilistic diffusion models in projected latent space. In *CVPR*, 2023. [3](#)
- [68] Lvmin Zhang and Maneesh Agrawala. Adding conditional control to text-to-image diffusion models. *arXiv preprint arXiv:2302.05543*, 2023. [2](#)
- [69] Daquan Zhou, Weimin Wang, Hanshu Yan, Weiwei Lv, Yizhe Zhu, and Jiashi Feng. Magicvideo: Efficient video generation with latent diffusion models. *arXiv preprint arXiv:2211.11018*, 2022. [1](#), [3](#)